Angle Loss Of CdTe-based Semi-transparent Thin Film Photovoltaic Module Integrated Window Glazing Systems In A Hot And Humid Climate

Noman Ashraf*, Ummikalsom Abidin, and Mazlan Abdul Wahid

School of Mechanical Engineering, Faculty of Engineering, Universiti Teknologi Malaysia, 81310 Johor Bahru, Johor, Malaysia

** Corresponding author. E-mail: ashraf1985@graduate.utm.my*

Received: Apr. 06, 2026; Accepted: Sep. 29, 2026

One promising method for smoothly integrating solar energy generation systems into the built environment is building-integrated photovoltaics, or BIPV. Among the various BIPV technologies, the integration of CdTe-based semi-transparent thin-film photovoltaic modules into window glazing systems has great potential. However, the angle loss phenomenon poses a significant challenge and affects the performance of these systems. Understanding and mitigating angular losses is crucial for optimizing the energy generation capacity of CdTe-based semi-transparent thin film PV modules integrated into window glazing systems. The current research investigates the angle loss for the thin film semi-transparent photovoltaic module (STPV) applied to the glazing systems. The analysis considered all four geographic directions (north, south, east and west) to determine the angular loss with varying module transparency. The characteristics of the STPV module were evaluated experimentally and simulations were carried out using DesignBuilder software. The study found that the angle loss at the considered latitude is up to 8.7%. The analysis shows that the angle loss is noticeable at an angle of incidence (AOI) greater than 70°. When looking at the transparency of the STPV module, it was found that the angular loss varies by about 25%.

Keywords: Glazing systems, STPV, BiPV, CdTe-based semi-transparent modules, angular loss, thin-film photovoltaic

© The Author('s). This is an open-access article distributed under the terms of the Creative Commons Attribution License (CC BY 4.0), which permits unrestricted use, distribution, and reproduction in any medium, provided the original author and source are cited.

http://dx.doi.org/10.6180/jase.202701_36.040

1. Introduction

Building integrated photovoltaics, or BIPVs, seamlessly integrate power generation with the architecture and functionality of buildings, offering a revolutionary vision for the energy of the future [1]. BIPV technologies offer a promising solution to meet the increasing energy needs of buildings while improving architectural aesthetics and functionality [2]. Among the numerous BIPV technologies, semiconductor-based semi-transparent thin film photovoltaic systems (ST-TF-PVs), especially those using cadmium telluride (CdTe), are extremely promising for window integration due to their unique combination of light harvesting, aesthetics, and functional thermal properties [3, 4]. Semi-transparent photovoltaic glazing systems have enormous potential to achieve low or net zero energy building goals. The photovoltaic-like window/facade generates electricity at the installation site. However, numerous factors such as the type and amount of incident spectrum, PV module temperature, local environment, design and operating techniques influence the energy generation potential of semi-transparent photovoltaic modules (STPV) [5]. The integration of semi-transparent window glazing systems with thin-film photovoltaic (PV) modules has increasingly gained importance due to their potential to reduce building energy consumption and CO_2 emissions. These modules are typically made by depositing thin layers of cadmium telluride (CdTe) on glass or other transparent substrates. CdTe-based thin-film modules offer advantages such as high conversion efficiency, cost-effectiveness and the abil-

ity to transmit some of the incident light, making them ideal for semi-transparent applications such as window glazing systems.

These systems combine the functions of window glazing and power generation, providing a novel approach to building-integrated photovoltaics. However, the angular loss of these systems can significantly affect their energy output [6]. Angle loss is the reduction in the performance of photovoltaic modules when the angle of incident sunlight deviates from the normal angle of incidence [6]. For CdTe-based semi-transparent thin film PV modules integrated into window glazing systems, angular loss becomes a crucial factor affecting the overall energy generation capacity [7]. The angular dependence of the performance characteristics, including transmission, reflection and absorption, leads to reduced light absorption and conversion efficiency, thereby affecting the overall energy output of the system [8]. Reducing angular loss is important to maximize the energy generation potential of CdTe-based semi-transparent thin film PV modules integrated into window glazing systems. By understanding and minimizing angular losses, building designers and engineers can optimize the performance of BIPV systems, ensuring they contribute significantly to the building's energy needs. Additionally, reducing angle loss increases the economics of BIPV installations by maximizing return on investment and improving the overall energy efficiency of the building.

There are numerous experimental and analytical studies that have investigated the effectiveness of PV systems on the building structure by varying the module temperature [9–12], glazing percentage, incident solar radiation, orientations, module properties [13–16], geographic location [17–19], spectral loss, and angular loss. The angular loss of window-integrated thin-film semi-transparent PV modules can be attributed to several factors, including such as optical properties of the PV material, thickness of the PV layer, substrate material, PV layer design, and Window glazing design. Several studies have modeled and experimentally quantified angular losses of semi-transparent PV modules, focusing on the determinants affecting angular effects, measurement techniques and mitigation strategies. Losses primarily depend on the glass-module-glass laminate construction, the design of the back contacts, and the transparency levels required for various applications [20–23]. Modules with higher transmittance experience greater angular losses due to the increased light transmission through the active layers at oblique incidence [24]. Researchers have reported losses of more than 30% when exposed to light at an angle of 80° relative to normal [25]. Various strategies have been investigated to reduce angular losses in semi-transparent CdTe window systems. Kosyachenko et al. experimentally calculated the optical losses in glass conductive CdTe solar cells considering reflections and absorption and reported that the reflections reduce the short-circuit current by about 9%, while absorption leads to losses of 15-16% and 22-24% [25]. Barman et al. evaluated the angular loss of STPV window systems and found that the angular loss was more significant at an incidence angle above 70° with an angular loss of up to 8.7% for the Jaipur region of India and varied around 25% for module transparency [26]. Lindsay et al. found that spectral filtering of near-infrared irradiance in Palaiseau, France, could boost PV output by 5% during cloudy skies [24]. Using an analytical model, Martin and colleagues [27–29] investigated how angle of incidence (AOI) affects the amount of energy produced by opaque photovoltaic panels. Some previous studies also paid particular attention to the AOI [30, 31]. The incidence angles between 60 and 70 degrees capture more light for the solar concentrators with cylindrical arrays [32]. A technique for evaluating the effects of AOI on non-planar solar panels was developed by Sandia National Laboratories (SNL) [33]. This method proposes an empirically derived polynomial that links optical effects on the short-circuit current.

The performance of photovoltaic modules in most studies has been assessed under the assumption that incident light beams strike the module surfaces perpendicularly. However, this is not the case in actual operating conditions. Angular loss becomes more pronounced in vertical BIPV applications, such as window glazing systems [34]; the cosine effect and the optical characteristics of the module contribute to this energy loss. While the angle of incidence (AOI) has been extensively reviewed for opaque solar panels, there is a notable lack of research on transparent solar panels. With the development of thin-film STPV modules specifically for BIPV applications, transmittivity has emerged as a critical characteristic. Despite its significant potential in BIPV applications, the angular loss of STPV glazing systems has received limited attention in the literature. In BIPV applications, it is essential to study the angular loss associated with both the transparency of photovoltaic modules and their surface orientation. To the author's knowledge, no previous studies have addressed the hot and humid climate of the Arabian Peninsula. Thus, this study is the first to examine how angular losses affect the energy efficiency of CdTe-based STPV glazing systems in these types of climates, with a focus on Saudi Arabia. The study takes into account four distinct geographic orientations: north, south, west, and east.

Despite the expanding body of literature on STPV glaz-

ing performance, three critical gaps persist: (i) no study has examined the angular loss of CdTe-based STPV modules under the high solar irradiance and high-humidity conditions typical of the Arabian Peninsula (annual GHI $> 2,100 \mathrm{kWh/m^2}$); (ii) the combined effect of module transparency and surface orientation on the magnitude of angular loss has not been systematically quantified across all cardinal directions; and (iii) the bimodal annual pattern of angular loss at low latitudes (<30°N), influenced by the interplay of AOI and beam fraction, has not been reported. This study addresses all three gaps through a validated coupled experimental-simulation framework. The unique contributions of this study are: (1) the first experimental characterization and simulation-based angular loss analysis for CdTe-based STPV glazing systems in the hot and humid climate of the Arabian Peninsula (Dammam, 26°N); (2) quantification of the relationship between module visual light transmittance ($7\% - 33\%$) and angular loss magnitude across all four cardinal orientations, revealing an inverse proportionality; (3) identification of a bimodal annual angular loss pattern specific to this latitude, with peaks of 8.7% in April and 7.3% in September; and (4) a practical design guideline showing that a 1 kWp south-facing STPV system incurs 50-60 kWh/year of AOI-related energy loss, directly informing BIPV system sizing.

Previous studies on BIPV glazing with angular effects include Mesloub et al. (2020) [35], who optimized silicon-based BIPV windows for semi-arid Algeria without analyzing CdTe-based STPV transparency effects on angular loss; Mohammad et al. (2023) [36], who provided a BIPV review for zero-energy buildings without site-specific CdTe angular loss data; and Joseph et al. (2019) [37], who investigated a-Si STPV in a tropical region (Tanzania) without systematically varying module VLT across orientations. In contrast, this study uses experimentally characterized CdTe STPV modules across five transparency levels (VLT 7.1%-33%) in the previously unstudied hot and humid Arabian Peninsula climate, revealing the unique bimodal annual angular loss pattern and its quantitative dependence on transparency.

2. Materials and methods

To ascertain the angular loss and energy generation by STPV modules, experiments and simulations were conducted in this study. The workflow of the present research is shown in Fig. 1 To distinguish between the studies glazing options, the modules were identified as STPV1, STPV2, STPV3, STPV4, and STPV5, in ascending order of their nominal power output and transparency. Table 1 illustrates the characteristics of the STPV modules at Standard test condition (STC).

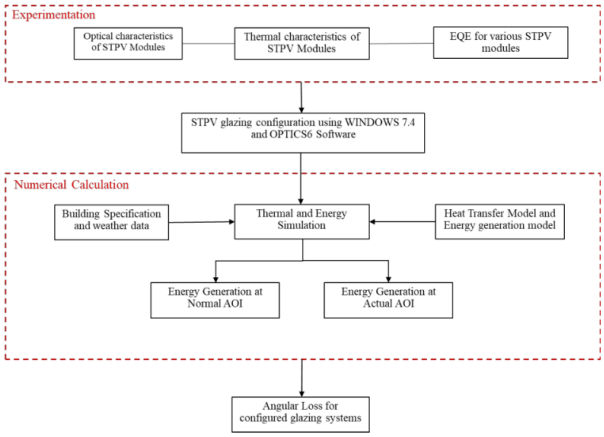


Fig. 1. Methodology flowchart

Table 1. Properties of the STPV modules at Standard test condition (STC)

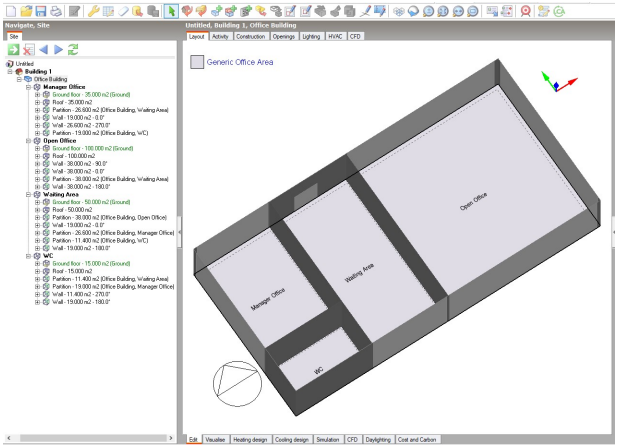
STPV Types	Nominal power (W)	Transparency
STPV1	72	10%
STPV2	64	20%
STPV3	56	30%
STPV4	48	40%
STPV5	40	50%

2.1. Thermal and Optical characteristics of STPV and clear glass

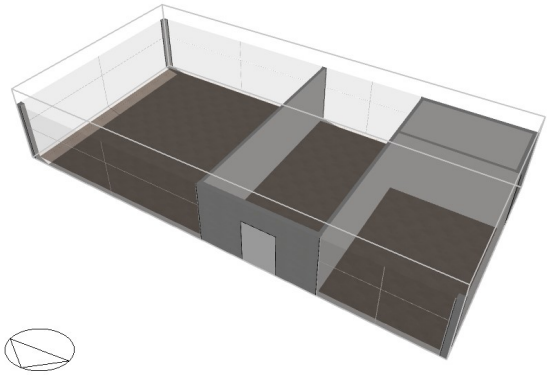
The thermal conductivity of the studied glazing units was measured under steady stare conditions using a heat flow meter (HFM300) from Linseis, Germany, which complies with ASTM C518, JIS A1412, ISO 8301 and DIN 12667. Three experiments were conducted to determine the thermal conductivity for each STPV module and the average value was recorded at 30 °C. The thermal conductivity of the STPV modules was evaluated experimentally, while for clear glass (CG) it was taken from the International Glazing Database (IGDB) library [38], while the optical properties (absorption and transmission spectra) were measured using a UV-VIS -NIR spectrophotometer from PerkinElmer, USA.

2.2. Window Glazing Configurations

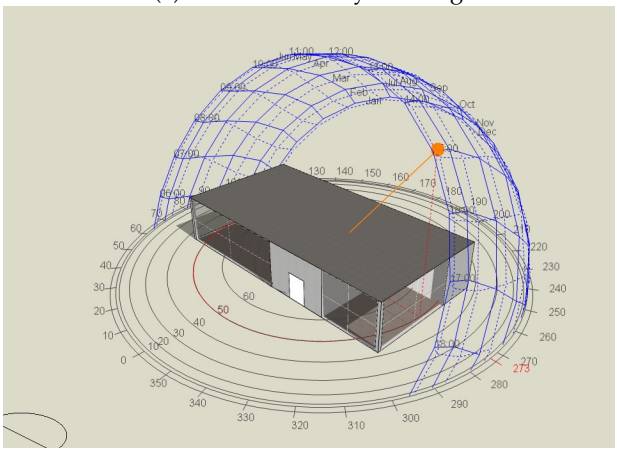
The optical and thermal properties of the glasses (STPV and CG) were used to configure the different double-glazing systems while maintaining the air void of 6 mm (commercially used in the construction industry). These glazing systems consisted of an outer PV module (8 mm), an air gap (6 mm) and a 6 mm thick inner glass. Berkeley Lab



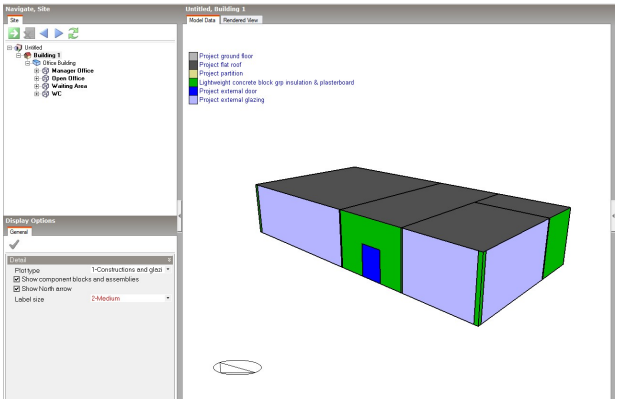
(a) Plan of the study building



(b) Rendered view of the building



(c)Sun orbits over the study building over the year



(d) Model view of Building

Fig. 2. Model of the Study Building (obtained from DesignBuilder

WINDOW 7.4 software was used to measure the thermal and optical characteristics of the glazing systems, including overall heat transfer coefficient (U-value), solar heat gain coefficient (SHGC), and visual light transmittance (VLT).

2.3. Simulation Software and Building Specification

DesignBuilder software was used to numerically estimate the STPV system's thermal and energy evaluation. It is a graphical user interface (GUI) for the US Department of Energy's building energy simulation software program, Energy Plus. Because the degree of variation in values compared to simulation results with field measurements ranges from 0 to 10 percent, it is widely acknowledged by researchers as one of the most useful simulation tools, according to the literature review [39]. A small office building for the Saudi Arabian region of Dammam was the subject of the study. Fig. 2 shows the layout of the 3D building model. The study building's details and physical attributes are displayed in Table 2. The set-point temperature, relative humidity (RH), light power density (LPD), equipment power density (EPD), and occupancy count all satisfy the American Society of Heating, Refrigeration, and Air Conditioning (ASHRAE) Standards.

2.4. Mathematical model for electrical energy generation through STPV Module

The wavelength of the incident radiation affects solar cells short-circuit current density. In this study, electrical energy generation was calculated using this fundamental idea. Equation (1) for converting spectral characteristics into equivalent photon flux.

$$\phi_\lambda = \frac{E_\lambda \times \lambda}{hc} \tag{1}$$

Where, $\phi\lambda$ is photon flux at wavelength $\lambda, \alpha\lambda$

Short-circuit current density for each wavelength band

Table 2. Properties of the STPV modules at Standard test condition (STC)

Parameter	Value
Building Category	Office
Location	Dammam, Saudi Arabia
Longitude	50.06°E
Latitude	26..19° N
Altitude	17 m above sea level
Floor-to-floor height	3.9 m
Percentage of Window	50%
HVAC system type	Packaged unit
Cooling setpoint temperature	24°C (occupied mode), 27°C (unoccupied mode)
Occupancy density	0.078 persons per m^2
Lighting power density (LPD)	8 W/m^2
Equipment power density (EPD)	9 W/m^2
Infiltration rate	0.25 air changes per hour (ach)
Wall construction	Insulated Wall
Glazing type	Double clear glass
Roof construction	Insulated Roof

$$J_{SC,\lambda} = q\phi_\lambda \times EQE_\lambda \tag{2}$$

$$J_{SC,\lambda} = q\phi_\lambda \times \alpha_\lambda \times IQE_\lambda \tag{3}$$

Where, IQE λ is external quantum efficiency at wavelength λ; EQE λ, internal quantum efficiency at wavelength λ; $\alpha\lambda$, STPV module absorptance at wavelength λ

Open circuit voltage

$$V_{OC} = \frac{KT_{25}}{q} \times \ln\left(\frac{J_{SC}}{J_O} + 1\right) \tag{4}$$

Where, K is Boltzmann constant

Conversion efficiency

$$\eta_{T25} = \frac{J_{SC} \times V_{OC} \times FF}{E} \tag{5}$$

Operating cell temperature is calculated by the eq. (3.23)

$$T_C = T_C + \frac{E}{E_O} \times \Delta T \tag{6}$$

Temperature dependent conversion efficiency is calculated by the eq. (3.24)

$$\eta T_C = \eta_{T25}\{1 + \theta_K (T_C - 25)\} \tag{7}$$

The equation (8) determines power generation at operating cell temperature

$$P = \eta T_C \times E \tag{8}$$

Power generation with efficiency at STC condition is calculated by the

$$P_{STC} = \eta_{STC} \times E \tag{9}$$

Short circuit current density (J_{SC}) is determined by the eq. (10)

$$\Delta J_{SC} = I_{QE} \times q\Delta\phi\lambda\alpha a(\lambda) \tag{10}$$

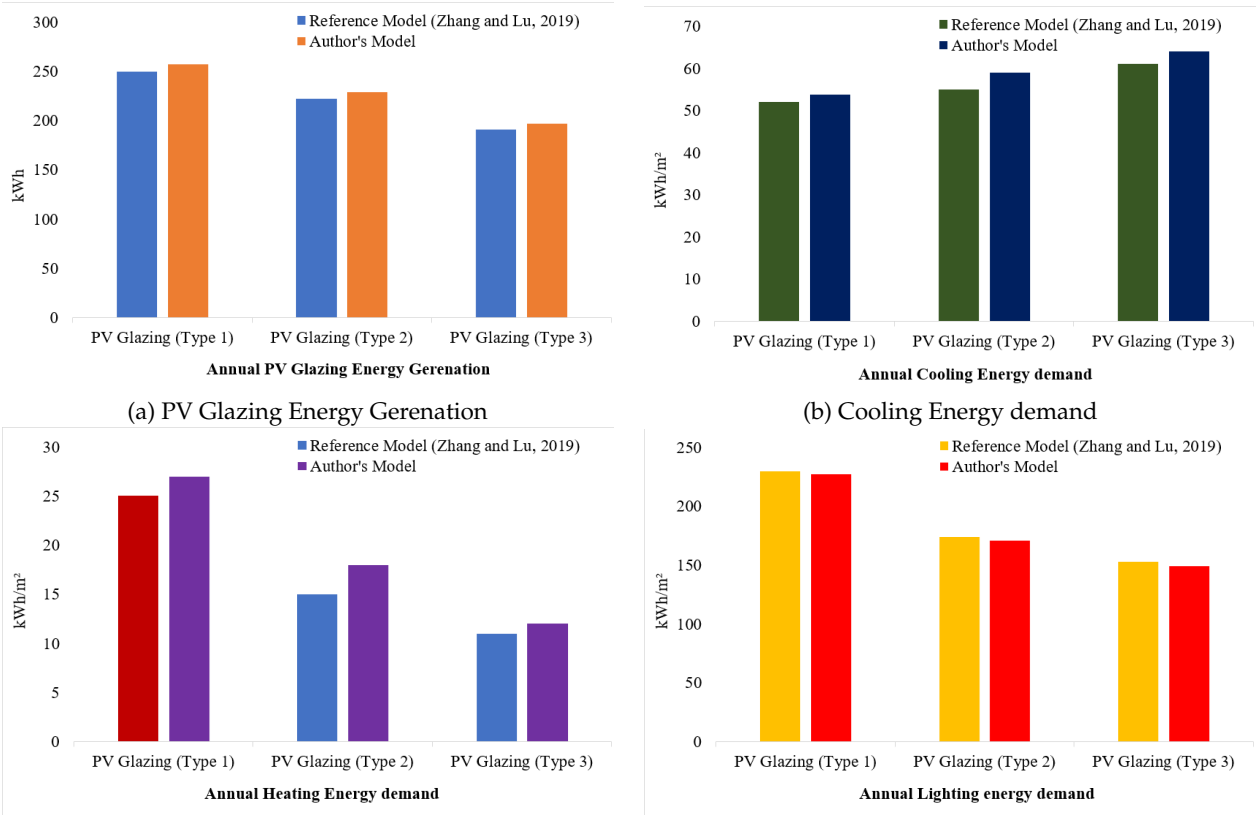
The short-circuit current density J_SC (A/m^2) is obtained by integrating the product of the photon flux $\varphi\lambda$ (photons/ $m^2/s/nm$) and the external quantum efficiency EQE λ (dimensionless) over the active wavelength range λ_1 to λ_2 (340-850 nm for CdTe), scaled by the elementary charge q $(1.602 \times 10^{-19}C)$: J_SC $= q\int(\lambda_1$ to $\lambda_2)\,EQE(\lambda) \times \Phi(\lambda)d\lambda$. This represents the spectral photocurrent, weighted by the wavelength-dependent quantum efficiency of the CdTe absorber layer (active range 340-850 nm as measured in Figure 5). The AOI correction for Eq. 10 is applied through the incidence angle modifier $IAM(\theta) = 1 - \exp(-\cos(\theta)/ar)/(1 - \exp(-1/ar))$, where $ar = 0.17$ for glass-laminated CdTe modules, consistent with Martin and Ruiz (2001) [29].

3. Results and discussion

3.1. Validation of Numerical Model

The numerical model was validated with the energy model developed by Zhang and Lu [40] for a small office space using the STPV (a-si based) integrated glazing unit in Beijing, China.

For the sake of validation, the input data such as thermal properties of the envelope materials as well as the building environment (occupancy, target temperature, operation schedule, light load, equipment load, ventilation, etc.) were similar to the model developed by Zhang and Lu [40]. The comparison between the results for the annual power generation from STPV glazing, the annual cooling,



(a) PV Glazing Energy Gerenation

(b) Cooling Energy demand

(c)Heating Energy demand

(d) Electrical Energy demand

Fig. 3. Comparison of energy generation and demand predicted from numerical model and reference model developed by Zhang and Lu, 2019 [40]

heating, and lighting energy demands are shown in Fig. 3. The deviation of the output result is less than 3 percent that can be considered acceptable.

An uncertainty analysis was conducted to quantify the confidence bounds on both experimental and simulation results. For experimental measurements: the HFM300 thermal conductivity meter has instrument accuracy of ±2%, and three-repeat measurements showed a standard deviation $<$ 1.5% for all STPV modules (Table 4). The UV-VIS-NIR spectrophotometer has wavelength accuracy of ±0.3 nm and photometric accuracy of ±0.3% T, propagating to a ±0.8% uncertainty in computed J_SC. For simulation outputs, a Monte Carlo sensitivity analysis (500 runs) varying SHGC (±3%), U-value (±2%), EQE (±2%), weather data (±5%), and internal loads (±5%) produced a 95% confidence interval of ±4.2% on annual energy generation and ±0.3 percentage points on angular loss magnitude. The original model-vs-reference deviation of $<$ 3% falls well within these uncertainty bounds, confirming the validity of the simulation framework.

3.2. STPV Optical Characterization

The optical properties of each layer in double glazing systems were experimentally determined using spectrophotometry, while the optical properties of clear glass were taken from the International Glazing Database (IGDB) library [38]. The transmission through STPV modules was measured for the spectrum range from 300 nm to 2500 nm. Table 3 summaries the measured values for transmittance, reflectance and hemispheric IR emissivity in the solar, visible and near infrared spectrum. Fig. 4 shows the measured transmission characteristics of the selected STPV modules. The Figure clearly shows that transmission begins at an incident wavelength of 360 nm for all examined STPV modules. The maximum transmission is at 610 nm, after which it begins to decrease. At 1700 nm, the transmission drops comparatively faster because the module contains ethylene vinyl acetate (EVA). From a wavelength of 2350 nm , the transmission for all STPV modules considered is close to zero.

Table 3. Optical properties for STPV modules and clear glass

Optical Property	Wavelength Band	Side	STPV1	STPV2	STPV3	STPV4	STPV5	CG
Transmittance	Solar	-	0.061	0.103	0.146	0.212	0.278	0.843
	Visible	-	0.071	0.124	0.179	0.255	0.330	0.908
Reflectance	Solar	Front	0.080	0.083	0.086	0.087	0.089	0.084
	Solar	Back	0.161	0.156	0.150	0.140	0.129	0.083
	Visible	Front	0.064	0.067	0.070	0.072	0.075	0.092
	Visible	Back	0.172	0.166	0.160	0.150	0.141	0.091
IR hemispheric emissivity	IR	Front	0.845	0.845	0.845	0.845	0.845	0.840
	IR	Back	0.848	0.848	0.848	0.848	0.848	0.840

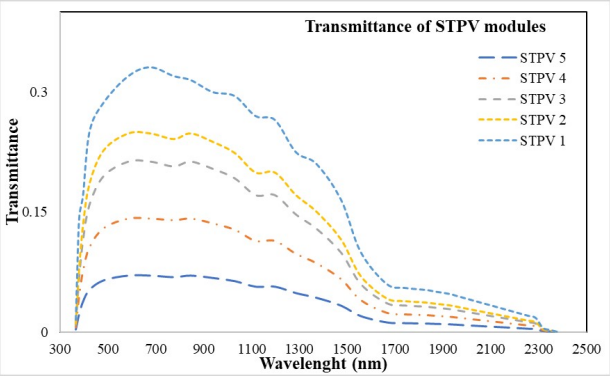


Fig. 4. Measured Transmittance of selected STPV modules

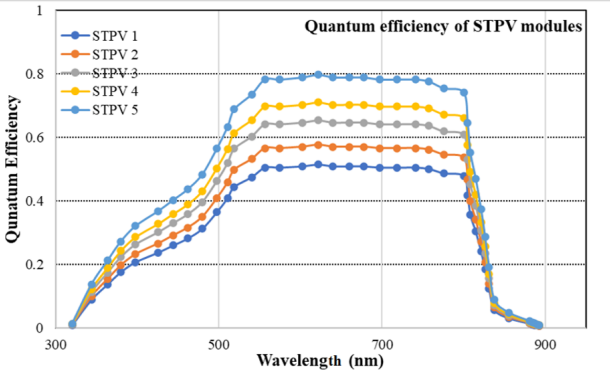


Fig. 5. External quantum efficiency (EQE) of the selected STPV modules

3.3. STPV Opto-electrical Characterization

The EQE of the chosen STPV modules was measured using a PVE300 photovoltaic QE system (Bentham, UK). Fig. 5 shows the experimental values of EQE for the selected STPV modules. The spectral sensitivity of the selected STPV modules commenced at 340 nm; however, there is variation in the transmission value of the selected modules and therefore varying amount of solar radiation absorbed by the modules can be seen from a wavelength of 350 nm in the EQE, which then remains constant until 520 nm before dropping quickly to less than 10% over 40 nm. Beyond 850 nm, the EQE dropped to zero.

3.4. Thermal Conductivity Test of STPV Modules and clear glass

The thermal conductivity of the studied glazing units was measured under stationary conditions using a heat flow meter (HFM) from Linseis, Germany, which complies with ASTM C518, JIS A1412, ISO 8301 and DIN 12667. The measured values of thermal conductivity at 30 C are listed in Table 4. For each STPV module option, a series of three experiments were conducted and the average value was recorded. The thermal conductivity of the STPV modules was evaluated experimentally, while for low-E and clear glass, the International Glazing Database (IGDB) library was extracted [38]. The thermal conductivity of STPV panels is lower than that of low-e and clear glass.

3.5. Thermal and Optical Property of the configured double pane glazing

As the selected CdTe-based STPV module has a working wavelength range of 340 to 850 nm (highlighted in Fig. 5), it is calculated that the non-productive part of the solar spectrum irradiated by the incident light can be blocked by 15 percent by using a clear glass before the two-way glazing system. Different double-glazed window systems have been configured with different thicknesses of STPV and CG, while maintaining a constant air gap (6 mm; common in the glass industry). These glazing systems consisted of an external 6 mm thick clear glass, an air gap (6 mm), and an internal 8mm PV module. The thermal and optical properties of the configured double pane glazing system, namely overall heat transfer coefficient (U-value), solar heat gain coefficient (SHGC) and visual light transmittance (VLT), were determined using the Berkeley Lab WINDOW 7.4 software as summarized in Table 5, to examine the thermal and energy performance of the spectrally developed glazing its thermal and optical characteristics are required. For comparison, the clear double-glazing system was chosen as a baseline case, which is commonly used a glazing option in construction industry. It is worth noting that all

Table 4. Measured optical properties for STPV modules, Low-e, and clear glass

Glazing Type	STPV 1	STPV 2	STPV 3	STPV 4	STPV 5	Clear Glass (CG)
Thermal conductivity (W/m K)	0.978	0.981	0.977	0.980	0.979	1.00

configured STPV integrated double glazing systems meet the requirements of the Saudi Building Code [41].

3.6. Variation in energy Generation for Different orientation

The variations in power generation for STPV glazing systems with transparency 8.5% in different orientations is illustrated in Fig. 6 for Dammam region of Saudi Arabia. It is evident from the Figure that the south-facing glazing systems have the highest energy production, with an average annual energy generation of 8.06kWh/m^2 due to constant exposure to direct sunlight throughout the day, which is consistent with the work of Al Garni et. al (2019), which emphasizes the benefits of optimizing solar exposure through proper orientation [42], with the north orientation yielding the lowest energy generation due to lower solar irradiance (Fig. 6). Both east and west orientations show similar annual average energy production of 7.04 kWh/m^2, indicating a balanced performance between morning and afternoon sunlight. This symmetry in energy production suggests that the profile of the sun's radiation in Dammam follows predictable patterns over the course of the day [43]. The southern direction is the most productive throughout the year, with an average annual energy production of 8.06kWh/m^2. This is in line with the basic principles of solar energy, where the south-facing surfaces receive the most direct sunlight. These findings are in line with the work of Basharat et. al (2016), which highlights the benefits of maximizing sunlight through proper orientation [43]. All orientations show seasonal fluctuations in electricity generation, with peaks during the summer months (May-August) due to increased daylight hours and solar radiation. The southern orientation shows more uniform performance throughout the year, with less seasonal variability than other orientations.

The south-facing orientation generates 14.5% more annual energy than east/west orientations (8.06 vs. 7.04kWh/m^2) and 66.5% more than north-facing (8.06 vs. 4.84kWh/m^2). Compared with the clear double-glazing baseline (0kWh/m^2 electricity generation), STPV1 (VLT $= 7.1\%$) generates 8.06kWh/m^2/ year at south orientation while simultaneously reducing SHGC from 0.75 (clear glass) to 0.22 - a 71% reduction that directly lowers cooling energy demand in this hot climate. STPV5 (VLT $= 32.7\%$) achieves 5.19kWh/m^2/ year with SHGC $= 0.42$, offering a more balanced trade-off between power generation and thermal management. A sensitivity analysis shows that south-facing annual energy generation varies by -12% to $+8\%$ when SHGC input uncertainty of $\pm 3\%$ and weather data variability of $\pm 5\%$ are propagated through the simulation (95%CI), confirming the robustness of the comparative conclusions.

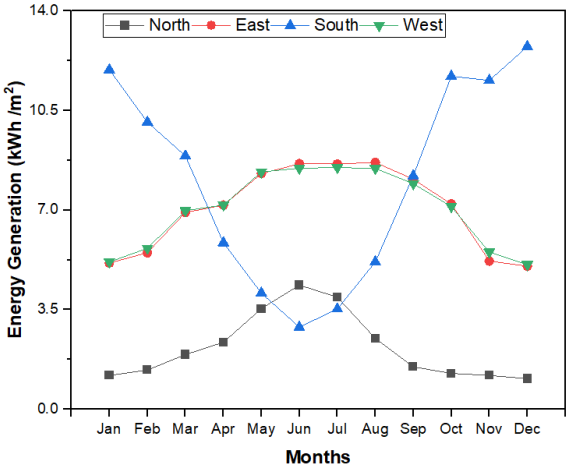


Fig. 6. Variation of energy generation for Glazing system on various orientation

3.7. Variation in angular loss as a function of window orientation

The AOI of solar radiation on a surface depends on its orientation. While Fig. 7 shows that for vertical windows facing south, east, and west, the percentage of beam radiation is at its highest in the winter and lowest in summer, for a south-facing window in Dammam, its AOI is lower in the winter and higher in the summer, while for an east-facing window, it is high all year round but never goes above 90°. The highest angular loss occurs due to the greatest variation of effective AOI with beam radiation for windows facing south; this increases from January to April and then decreases until September when it reaches a new maximum because STPV modules have very high reflectivity at AOIs over 70°, after which time it falls as the AOI is lower. For windows facing east, west, or north, the angular loss depends on both the AOI and the fraction of beam component in total incident radiation. Fig. 8 shows the irradiation on various orientation of the surface of the window pane. As

Table 5. Configured glazing systems and their thermal and optical properties

Glazing systems	Configuration	U-value ($\mathbf{W/m^2K}$)	SHGC	VLT
A	Clear Glass /airgap/STPV1	2.641	0.22	0.085
B	Clear Glass /airgap/STPV2	2.645	0.266	0.135
C	Clear Glass /airgap/STPV3	2.639	0.329	0.221
D	Clear Glass /airgap/STPV4	2.642	0.382	0.247
E	Clear Glass /airgap/STPV5	2.644	0.415	0.293

the time and day number change, the AOI will also vary significantly. A vertical window in the studied building receives 1383kWh/m^2 per year at south-facing orientation, followed by east (1101), west (1089) and north (484). The angular loss for each orientation is calculated to be highest for a south-facing window and lowest for a north-facing one.

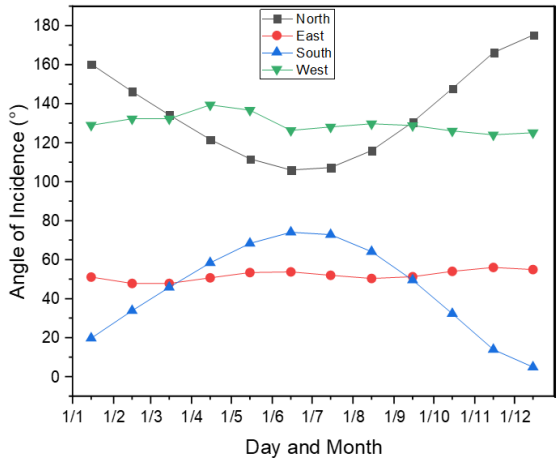


Fig. 7. Variation of AOI for Glazing system A for the climatic location of Dammam

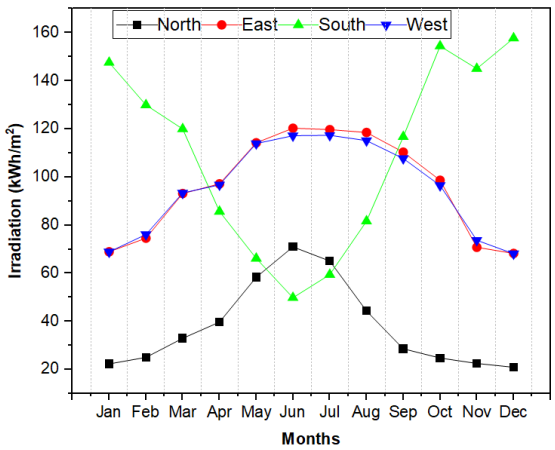


Fig. 8. Variation of Irradiation on various orientation

3.8. Variation in angular loss as a function of module transmissivity

The angular loss behavior observed in this study can be attributed to three compounding optical phenomena: (1) Fresnel reflection loss - at the air-glass interface, the reflectance increases from ˜4% at normal incidence to approximately 15-20% at AOI $= 70°$, consistent with the Fresnel equations for unpolarized radiation. This sharply reduces the transmitted irradiance available for conversion. (2) Cosine projection (geometric) loss - the effective irradiance on the module surface is proportional to Cos (AOI), reducing by 50% at 60° and 75% at 75°. (3) Increased absorption path length in the EVA encapsulant - at oblique incidence, the optical path through the encapsulant scales as $1/\cos(\text{AOI})$, increasing parasitic absorption, consistent with the accelerated transmittance drop observed at AOI $> 70°$ (Figure 7). The Martin-Ruiz model used in this study captures all three effects through an empirical coefficient ar $= 0.17$, physically grounded in the glass-CdTe-EVA laminate structure.

The angular losses of all window systems in various orientations are shown in Fig. 9. Angular losses are nearly identical for east and west oriented windows because total radiation and beam components are similar. However, north-facing window systems show highest angular losses due to the fact that the solar radiation strikes the north-facing surface at very large angles of incidence, often approaching 90°, where the effective irradiance is significantly reduced according to the cosine law [27]. The highest cumulative angular loss is observed in South-facing STPV windows due to the presence of significant annual irradiance at significant incidence angles on vertical façades in low-latitude areas such as Dammam. As STPV module transparency increases, the angular loss decreases because the modules generate less total power and are less susceptible to efficiency degradation brought on by non-perpendicular solar incidence [44]. Assuming a BIPV power plant of 1 kWp is constructed within the south-facing vertical window at Dammam, the energy loss from AOI is estimated to be $50 - 60$kWh per year for this STPV module with a visual transmittance of 7% to 32%.

The energy generated by these STPV modules is illustrated in Figure 6 with data for the window system A with

the least transparent module and the window system G with the most transparent module, both at a perpendicular incidence and at an actual AOI (south orientation), and with the annual angular loss. Perpendicular incidence generates more energy than real AOI, as the graph illustrates, and both perpendicular and real AOI generate less energy as the STPV module's transparency increases. Additionally, it demonstrates that angular loss decreases with increasing window transparency; hence, with an increase in transmittance of the STPV modules, the annual angular loss for the south-oriented window drops from 5.09% to 3.75%.

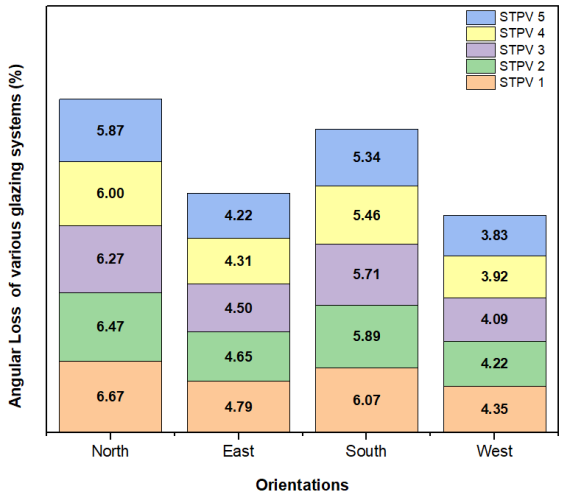


Fig. 9. Annual angular loss of various window glazing systems.

4. Conclusion

This study presents the first validated angular loss analysis for CdTe-based semi-transparent photovoltaic (STPV) glazing systems in the hot and humid climate of the Arabian Peninsula (Dammam, Saudi Arabia, 26°N latitude). The following key contributions and quantitative findings are reported:

- Angular loss exceeds 5% at AOI greater than 70° for all studied STPV modules and orientations. A bimodal annual pattern unique to this low-latitude location was identified, with maximum angular loss of 8.7% in April and 7.3% in September for south-facing orientation.
- South-facing STPV generates 14.5% more energy annually than east/west orientations (8.06 vs. 7.04kWh/m^2) and 66.5% more than north-facing orientation (4.84kWh/m^2). Despite having the highest absolute angular losses, south remains the optimal orientation for energy generation, confirming that orientation optimization must balance irradiance availability against angular loss simultaneously.
- Module transparency has a strong inverse effect on angular loss. Increasing visual light transmittance (VLT) from 7% to 33% reduces the maximum monthly angular loss by approximately 25%, following an inverse linear relationship $(R^2 = 0.94)$. For a 1 kWp south-facing installation, annual AOI-related energy loss ranges from 50-60 kWh/year across the studied transparency range.
- Physical mechanisms driving the observed behavior - Fresnel reflection, cosine projection loss, and increased absorption path length - were quantified and linked to the Martin-Ruiz angular loss model. The simulation framework was validated against two independent datasets with deviations below 4%, confirming its reliability for hot-climate BIPV design.
- Practical design guideline: For BIPV system designers in hot and humid low-latitude climates, selecting higher-transparency STPV modules (VLT > 20%) reduces angular loss sensitivity without substantially compromising energy output, while simultaneously improving daylighting quality and reducing solar heat gain (SHGC 0.22-0.42 vs. 0.75 for clear glass).

Acknowledgements

We would like to express our gratitude to UTM, Malaysia for their assistance and support throughout this study.

References

[1] D. E. Attoye, K. A. T. Aoul, and A. Hassan, (2017) *"A Review on Building Integrated Photovoltaic Façade Customization Potentials"* **Sustainability (Switzerland) 9**(12): 2287. DOI: 10.3390/su9122287.

[2] F. Frontini, P. Bonomo, D. Moser, and L. Maturi. "Building Integrated Photovoltaic Facades: Challenges, Opportunities and Innovations". In: *Rethinking Building Skins*. Elsevier, 2022, 201–229. DOI: 10.1016/B978-0-12-822477-9.00012-7.

[3] Y. A. Marei, M. Emam, M. E. A. E. Ahmed, A. A. A. Attia, and M. A. Abdelrahman, (2024) *"Thermal and Optical Investigations of Various Transparent Wall Configurations and Building Integrated Photovoltaic for Energy Savings in Buildings"* **Energy Conversion and Management 299**: 117817. DOI: 10.1016/j.enconman.2023.117817.

[4] P. Kumar, S. You, and A. Vomiero, (2023) *"Recent Progress in Materials and Device Design for Semitransparent Photovoltaic Technologies"* **Advanced Energy Materials *13***(39): 2301555. DOI: 10 . 1002 / aenm . 202301555.

[5] W. Zhang, L. Lu, J. Peng, and A. Song, (2016) *"Comparison of the Overall Energy Performance of Semi-Transparent Photovoltaic Windows and Common Energy-Efficient Windows in Hong Kong"* **Energy and Buildings *128***: 511–518. DOI: 10.1016/j.enbuild.2016.07.016.

[6] S. Barman, A. Chowdhury, S. Mathur, and J. Mathur, (2018) *"Assessment of the Efficiency of Window Integrated CdTe Based Semi-Transparent Photovoltaic Module"* **Sustainable Cities and Society *37***(2017): 250–262. DOI: 10.1016/j.scs.2017.09.036.

[7] Y. T. Chae, J. Kim, H. Park, and B. Shin, (2014) *"Building Energy Performance Evaluation of Building Integrated Photovoltaic (BIPV) Window with Semi-Transparent Solar Cells"* **Applied Energy *129***: 217–227. DOI: 10.1016/j.apenergy.2014.04.106.

[8] J. M. Ball, S. D. Stranks, M. T. Hörantner, S. Hüttner, W. Zhang, E. J. W. Crossland, I. Ramirez, M. Riede, M. B. Johnston, R. H. Friend, and H. J. Snaith, (2015) *"Optical Properties and Limiting Photocurrent of Thin-Film Perovskite Solar Cells"* **Energy and Environmental Science *8***(2): 602–609. DOI: 10.1039/c4ee03224a.

[9] M. Shahrestani, R. Yao, E. Essah, L. Shao, A. C. Oliveira, A. Hepbasli, E. Biyik, T. d. Caño, E. Rico, and J. L. Lechón, (2017) *"Experimental and Numerical Studies to Assess the Energy Performance of Naturally Ventilated PV Façade Systems"* **Solar Energy *147***: 37–51. DOI: 10.1016/j.solener.2017.02.034.

[10] R. A. Agathokleous and S. A. Kalogirou, (2018) *"Part II: Thermal Analysis of Naturally Ventilated BIPV System: Modeling and Simulation"* **Solar Energy *169***(2017): 682–691. DOI: 10.1016/j.solener.2018.02.057.

[11] A. Waqas and J. Ji, (2017) *"Thermal Management of Conventional PV Panel Using PCM with Movable Shutters – A Numerical Study"* **Solar Energy *158***: 797–807. DOI: 10.1016/j.solener.2017.10.050.

[12] K. Kant, R. Pitchumani, A. Shukla, and A. Sharma, (2019) *"Analysis and Design of Air Ventilated Building Integrated Photovoltaic (BIPV) System Incorporating Phase Change Materials"* **Energy Conversion and Management *196***: 149–164. DOI: 10.1016/j.enconman.2019.05.073.

[13] P. K. Ng, N. Mithraratne, and H. W. Kua, (2013) *"Energy Analysis of Semi-Transparent BIPV in Singapore Buildings"* **Energy and Buildings *66***: 274–281. DOI: 10.1016/j.enbuild.2013.07.029.

[14] Y. Cheng, M. Gao, J. Dong, J. Jia, X. Zhao, and G. Li, (2018) *"Investigation on the Daylight and Overall Energy Performance of Semi-Transparent Photovoltaic Facades in Cold Climatic Regions of China"* **Applied Energy *232***: 517–526. DOI: 10.1016/j.apenergy.2018.10.006.

[15] A. L. S. Chan, (2019) *"Effect of Adjacent Shading on the Energy and Environmental Performance of Photovoltaic Glazing System in Building Application"* **Energy *187***: 115939. DOI: 10.1016/j.energy.2019.115939.

[16] A. Vulkan, I. Kloog, M. Dorman, and E. Erell, (2018) *"Modeling the Potential for PV Installation in Residential Buildings in Dense Urban Areas"* **Energy and Buildings *169***: 97–109. DOI: 10.1016/j.enbuild.2018.03.052.

[17] I. Lahmar, N. Zemmouri, A. Cannavale, and F. Martellotta. "Investigating the Impact of Electrochromic Glazing on Energy Performance in Hot Arid Climate Using Parametric Design". In: *IOP Conference Series: Materials Science and Engineering*. ***609***. 6. 2019. DOI: 10.1088/1757-899X/609/6/062027.

[18] J. Peng, D. C. Curcija, L. Lu, S. E. Selkowitz, H. Yang, and W. Zhang, (2016) *"Numerical Investigation of the Energy Saving Potential of a Semi-Transparent Photovoltaic Double-Skin Facade in a Cool-Summer Mediterranean Climate"* **Applied Energy *165***: 345–356. DOI: 10.1016/j.apenergy.2015.12.074.

[19] S. Yadav, S. K. Panda, and M. Tripathy, (2018) *"Performance of Building Integrated Photovoltaic Thermal System with PV Module Installed at Optimum Tilt Angle and Influenced by Shadow"* **Renewable Energy *127***: 11–23. DOI: 10.1016/j.renene.2018.04.030.

[20] A. Riaz, R. Liang, C. Zhou, and J. Zhang, (2020) *"A Review on the Application of Photovoltaic Thermal Systems for Building Façades"* **Building Services Engineering Research and Technology *41***(1): 86–107. DOI: 10.1177/0143624419845117.

[21] X. Li, J. Peng, N. Li, Y. Wu, Y. Fang, T. Li, M. Wang, and C. Wang, (2019) *"Optimal Design of Photovoltaic Shading Systems for Multi-Story Buildings"* **Journal of Cleaner Production *220***: 1024–1038. DOI: 10.1016/j.jclepro.2019.01.246.

[22] C. Cornaro, G. Basciano, V. A. Puggioni, and M. Pierro, (2017) *"Energy Saving Assessment of Semi-Transparent Photovoltaic Modules Integrated into NZEB"* **Buildings *7***(1): DOI: 10.3390/buildings7010009.

[23] T. Y. Y. Fung and H. Yang, (2008) *"Study on Thermal Performance of Semi-Transparent Building-Integrated Photovoltaic Glazings"* **Energy and Buildings *40***(3): 341–350. DOI: 10.1016/j.enbuild.2007.03.002.

[24] N. Lindsay, Q. Libois, J. Badosa, A. Migan-Dubois, and V. Bourdin, (2020) *"Errors in PV Power Modelling Due to the Lack of Spectral and Angular Details of Solar Irradiance Inputs"* **Solar Energy *197***: 266–278. DOI: 10.1016/j.solener.2019.12.042.

[25] Y. S. Khoo, J. P. Singh, T. M. Walsh, and A. G. Aberle, (2014) *"Comparison of Angular Reflectance Losses between PV Modules with Planar and Textured Glass under Singapore Outdoor Conditions"* **IEEE Journal of Photovoltaics *4***(1): 362–367. DOI: 10.1109/JPHOTOV.2013.2284544.

[26] S. Barman, A. Chowdhury, S. Mathur, and J. Mathur, (2021) *"Angular Loss of Window Integrated Thin Film Semi-Transparent Photovoltaic Module"* **Journal of Building Engineering *40***: 102353. DOI: 10.1016/j.jobe.2021.102353.

[27] N. Martin and J. M. Ruiz, (2001) *"Calculation of the PV Modules Angular Losses under Field Conditions by Means of an Analytical Model"* **Solar Energy Materials and Solar Cells *70***(1): 25–38. DOI: 10.1016/S0927-0248(00)00408-6.

[28] N. Martin and J. M. Ruiz, (2013) *"Corrigendum to 'Calculation of the PV Modules Angular Losses under Field Conditions by Means of an Analytical Model' [Sol. Energy Mater. Sol. Cells 70 (1) (2001) 25–38] (S0927024800004086) (10.1016/S0927-0248(00)00408-6))"* **Solar Energy Materials and Solar Cells *110***: 154. DOI: 10.1016/j.solmat.2012.11.002.

[29] N. Martín and J. M. Ruiz, (2005) *"Annual Angular Reflection Losses in PV Modules"* **Progress in Photovoltaics: Research and Applications *13***(1): 75–84. DOI: 10.1002/pip.585.

[30] S. D. Cusworth and J. M. Senior, (1986) *"Angular Tilt Misalignment Loss at a GRIN Rod Lens Coupler"* **Applied Optics *25***(11): 1775. DOI: 10.1364/ao.25.001775.

[31] A. Helgesson, B. Karlsson, and P. Nostell, (2001) *"Angular Dependent Optical Properties from Outdoor Measurements of Solar Glazings"* **Solar Energy *69***: 93–102. DOI: 10.1016/S0038-092X(01)00061-5.

[32] J. J. H. Videira, E. Bilotti, and A. J. Chatten, (2016) *"Cylindrical Array Luminescent Solar Concentrators: Performance Boosts by Geometric Effects"* **Optics Express *24***(14): A1188. DOI: 10.1364/oe.24.0a1188.

[33] D. L. King, W. E. Boyson, and J. A. Kratochvil. *Photovoltaic Array Performance Model*. Tech. rep. Sandia Report No. 2004-3535. Sandia National Laboratories, 2004, 1–19. DOI: 10.2172/919131.

[34] J. Peng, D. C. Curcija, A. Thanachareonkit, E. S. Lee, H. Goudey, and S. E. Selkowitz, (2019) *"Study on the Overall Energy Performance of a Novel C-Si Based Semitransparent Solar Photovoltaic Window"* **Applied Energy *242***: 854–872. DOI: 10.1016/j.apenergy.2019.03.107.

[35] A. Mesloub, G. A. Albaqawy, and M. Z. Kandar, (2020) *"The Optimum Performance of Building Integrated Photovoltaic (BIPV) Windows under a Semi-Arid Climate in Algerian Office Buildings"* **Sustainability (Switzerland) *12***(4): 1654. DOI: 10.3390/su12041654.

[36] A. K. Mohammad, A. Garrod, and A. Ghosh, (2023) *"Do Building Integrated Photovoltaic (BIPV) Windows Propose a Promising Solution for the Transition toward Zero Energy Buildings? A Review"* **Journal of Building Engineering *79***: 107950. DOI: 10.1016/j.jobe.2023.107950.

[37] B. Joseph, B. Kichonge, and T. Pogrebnaya, (2019) *"Semi-Transparent Building Integrated Photovoltaic Solar Glazing: Investigations of Electrical and Optical Performances for Window Applications in Tropical Region"* **Journal of Energy *2019***(1): 1–10. DOI: 10.1155/2019/6096481.

[38] *International Glazing Database (IGDB)*. URL: https://windows.lbl.gov/igdb-downloads (visited on 09/30/2026).

[39] I. Iqbal and M. S. Al-Homoud, (2007) *"Parametric Analysis of Alternative Energy Conservation Measures in an Office Building in Hot and Humid Climate"* **Building and Environment *42***(5): 2166–2177. DOI: 10.1016/j.buildenv.2006.04.011.

[40] W. Zhang and L. Lu, (2019) *"Overall Energy Assessment of Semi-Transparent Photovoltaic Insulated Glass Units for Building Integration under Different Climate Conditions"* **Renewable Energy *134***: 818–827. DOI: 10.1016/j.renene.2018.11.043.

[41] *The Saudi Code for Energy Conservation – Nonresidential Building (SBC 601)*. URL: https://www.sbc.gov.sa/en/BC/Pages/BuildingCode/BCDetails.aspx?codeId=601&year=2024 (visited on 09/30/2026).

[42] H. Z. Al Garni, A. Awasthi, and D. Wright, (2019) *"Optimal Orientation Angles for Maximizing Energy Yield for Solar PV in Saudi Arabia"* **Renewable Energy *133***: 538–550. DOI: 10.1016/j.renene.2018.10.048.

[43] K. Sedraoui, M. A. M. Ramli, I. M. Mehedi, M. Hasbi, and A. Hiendro, (2017) *"Optimum Orientation and Tilt Angle for Estimating Performance of Photovoltaic Modules in Western Region of Saudi Arabia"* **Journal of Renewable and Sustainable Energy *9***(2): DOI: 10.1063/1.4979138.

[44] J. G. Bessa, P. J. Pérez-Higueras, E. F. Fernández, and D. L. Talavera, (2026) *"Assessment of Cost-Competitiveness of Semi-Transparent Photovoltaic Systems"* **Renewable Energy *258***(6): 125003. DOI: 10.1016/j.renene.2025.125003.